

Abstract

The 1-D saltation-abrasion model of channel bedrock incision of Sklar and Dietrich, in which the erosion rate is buffered by the surface area fraction of bedrock covered by alluvium, was a major advance over models that treat river erosion as a function of bed slope and drainage area. Their model is, however, limited because it calculates bed cover in terms of bedload sediment supply rather than local bedload transport. It implicitly assumes that as sediment supply from upstream changes, the transport rate adjusts instantaneously everywhere downstream to match. This assumption is not valid in general, and thus can give rise unphysical consequences. Here we present a unified morphodynamic formulation of both channel incision and alluviation which specifically tracks the spatiotemporal variation of both bedload transport and alluvial thickness. It does so by relating the cover fraction not to a ratio of bedload supply rate to capacity bedload transport, but rather to the ratio of alluvium thickness to a macro-roughness characterizing the bedrock surface. The new formulation predicts waves of alluviation and rarification, in addition to bedrock erosion. Embedded in it are three physical processes: alluvial diffusion, fast downstream advection of alluvial disturbances and slow upstream migration of incisional disturbances. Solutions of this formulation over a fixed bed are used to demonstrate the stripping of an initial alluvial cover, the emplacement of alluvial cover over an initially bare bed and the advection–diffusion of a sediment pulse over an alluvial bed. A solution for alluvial-incisional interaction in a channel with a basement undergoing net rock uplift shows how an impulsive increase in sediment supply can quickly and completely bury the bedrock under thick alluvium, so blocking bedrock erosion. As the river responds to rock uplift or base level fall, the transition point separating an alluvial reach upstream from an alluvial-bedrock reach downstream migrates upstream in the form of a “hidden knickpoint”. A solution for the case of a zone of rock subsidence (graben) bounded upstream and downstream by zones of rock uplift (horsts) yields a steady-state solution that is unattainable with the original saltation-abrasion model. A solution for the case of bedrock-alluvial coevolution upstream of an

Macro-roughness model of bedrock-alluvial river morphodynamics

L. Zhang et al.

Title Page

Abstract

Introduction

Conclusions

References

Tables

Figures



Back

Close

Full Screen / Esc

Printer-friendly Version

Interactive Discussion



alluviated river mouth illustrates how the bedrock surface can be progressive buried not far below the alluvium. Because the model tracks the spatiotemporal variation of both bedload transport and alluvial thickness, it is applicable to the study of the incisional response of a river subject to temporally varying sediment supply. It thus has the potential to capture the response of an alluvial-bedrock river to massive impulsive sediment inputs associated with landslides or debris flows.

1 Introduction

The pace of river-dominated landscape evolution is set by the rate of downcutting into bedrock across the channel network. The coupled process of river incision and hillslope response is both self-promoting and self-limiting (Gilbert, 1877). Low rates of incision entail some sediment supply from upstream hillslopes, which provides a modicum of abrasive material in river flows that further facilitates bedrock channel erosion. Faster downcutting leads to higher rates of hillslope sediment supply, boosting the concentration of erosion “tools” and bedrock wear rates, but also leading to greater cover of the bedrock bed with sediment (Sklar and Dietrich, 2001, 2004, 2006; Turowski et al., 2007; Lamb et al., 2008; Turowski, 2009). Too much sediment supply leads to choking of the channels by alluvial cover and the retardation of further channel erosion (e.g., Stark et al., 2009). This competition between incision and sedimentation leads long-term eroding channels to typically take a mixed bedrock-alluvial form in which the pattern and depth of sediment cover fluctuate over time in apposition to the pattern of bedrock wear.

Theoretical approaches to treating the erosion of bedrock rivers have shifted over recent decades (see Turowski (2012) for a recent review). The pioneering work of Howard and Kerby (1983) focused on bedrock channels with little sediment cover; it led to the detachment-limited model of Howard (1994) in which channel erosion is treated as a power function of river slope and characteristic discharge, and the “stream-power-law” approach in which the power-law scaling of channel slope with upstream area

Macro-roughness model of bedrock-alluvial river morphodynamics

L. Zhang et al.

Title Page

Abstract

Introduction

Conclusions

References

Tables

Figures



Back

Close

Full Screen / Esc

Printer-friendly Version

Interactive Discussion



rather than local sediment transport. The model is thus unable to capture the interaction between processes that drive evolution of an alluvial bed and those that drive the evolution of an incising of bedrock-alluvial bed. Second, for related reasons, it cannot account for bedrock topography significant enough to affect the pattern of sediment storage and rock exposure. Such a topography is illustrated in Fig. 1 for the Shimanto River, Japan.

Here we address both these challenges in a model that allows both alluvial and incisional processes to interact and co-evolve. We do this by relating the cover factor geometrically to a measure of bedrock topography, here called macro-roughness, rather than to the ratio of sediment supply rate to capacity sediment transport rate. Our model encompasses downstream advective alluvial behavior (e.g., waves of alluvium), diffusive alluvial behavior and upstream advecting incisional behavior (e.g., knickpoint migration). In order to distinguish between the model of Sklar and Dietrich (2004, 2006) and the present model, we refer to the former as the CSA (Capacity-based Saltation-Abrasion) model, and the latter as the MRSAA (Macro-Roughness-based Saltation-Abrasion-Alluviation) model.

2 Capacity-based Saltation-Abrasion (CSA) geomorphic incision law and its implications for channel evolution: upstream-migrating waves of incision

2.1 CSA geomorphic incision law

Sklar and Dietrich (2004, 2006) present the following model, referred to here as the Capacity-based Saltation-Abrasion (CSA) model, for bedrock incision in mixed bedrock-alluvial rivers transporting gravel. Defining E as the vertical rate of incision into bedrock, q_b as the volume gravel transport rate per unit width (specified in their model solely in terms of a supply, or feed rate q_{bf}) and q_{bc} as the capacity volume

Macro-roughness model of bedrock-alluvial river morphodynamics

L. Zhang et al.

Title Page

Abstract

Introduction

Conclusions

References

Tables

Figures

◀

▶

◀

▶

Back

Close

Full Screen / Esc

Printer-friendly Version

Interactive Discussion



where D is gravel clast size, D_u is an upstream value of D , x is downstream distance and α_d is a diminution coefficient. If all diminution results from abrasion, α_d is related to β as

$$\alpha_d = \frac{\beta}{3} \quad (4a)$$

In the case of constant β , and therefore α_d , the distance L_{half} for such a clast to halve in size is given as

$$L_{\text{half}} = \frac{\ln(2)}{\alpha_d} \quad (4b)$$

This interpretation of abrasion coefficient β in terms of diminution coefficient α_d allows comparison of the experimental results of Sklar and Dietrich (2001) with values of α_d previously obtained from abrasion mills (Parker, 2008: see Fig. 3-41 therein; Kodama, 1994).

The relations of Sklar and Dietrich (2004, 2006) to compute β and q_{bc} can be cast in the following form:

$$\beta = \frac{0.08\rho_s RgY}{k_v\sigma_t^2} \left(\frac{\tau^*}{\tau_c^*} - 1\right)^{-1/2} \left[1 - \frac{\tau^*}{R_f^2}\right]^{3/2} \quad (5a)$$

$$R_f = \frac{v_s}{\sqrt{RgD}} \quad (5b)$$

$$q_{bc} = \alpha_b \sqrt{RgD} D (\tau^* - \tau_c^*)^{n_b} \quad (5c)$$

In the above relations, D corresponds to the characteristic size of the gravel clasts that are effective in abrading the bedrock, ρ_s is the material density of the clasts, R is their submerged specific gravity (~ 1.65 for quartz), g is gravitational acceleration, τ^* is the dimensionless Shields number of the flow, τ_c^* is the threshold Shields number

**Macro-roughness
model of
bedrock-alluvial river
morphodynamics**

L. Zhang et al.

Title Page

Abstract

Introduction

Conclusions

References

Tables

Figures

◀

▶

◀

▶

Back

Close

Full Screen / Esc

Printer-friendly Version

Interactive Discussion



for the onset of significant bedload transport, α_b and n_b denote, respectively, relation-specific dimensionless coefficient and exponent, v_s is the fall velocity corresponding to size D , Y is the bedrock modulus of elasticity, σ_t is the rock tensile strength, and k_v is a dimensionless coefficient of the order of 1×10^{-6} . (In the above two relations and the text, several misprints in Sklar and Dietrich, (2004, 2006) have been corrected on the advice of the authors.) Equation (5c) corresponds to the bedload transport relation of Fernandez Luque and van Beek (1976) when $\alpha_b = 5.7$ and $n_b = 1.5$; Sklar and Dietrich (2004, 2006) used this relation with the assumed value $\tau_c^* = 0.03$.

It is useful to cast Eq. (5c) in the form

$$\beta = \beta_r \frac{\left(\frac{\tau^*}{\tau_c} - 1\right)^{-1/2} \left[1 - \frac{\tau^*}{R_f^2}\right]^{3/2}}{\left(\frac{\tau_f^*}{\tau_c} - 1\right)^{-1/2} \left[1 - \frac{\tau_f^*}{R_f^2}\right]^{3/2}} \quad (5d)$$

where β_r is a reference value of β , either computed from known values of the parameters Y , k_v , σ_t , R_f etc., or estimated indirectly.

2.2 Embedding of CSA into a model of bedrock surface evolution

A relation for the evolution of bedrock surface elevation η_b is obtained by substituting the CSA geomorphic law for incision of Eq. (1b) into a simplified 1-D mass conservation equation for bedrock material subjected to piston-style rock uplift or base level fall (Sklar and Dietrich, 2006):

$$\frac{\partial \eta_b}{\partial t} = v - l_f \beta q_{bc} \rho_c (1 - \rho_c) \quad (6)$$

Here t denotes time, v denotes the relative vertical velocity between the rock underlying the channel (which is assumed to undergo no deformation) and the point at which base

**Macro-roughness
model of
bedrock-alluvial river
morphodynamics**

L. Zhang et al.

Title Page

Abstract

Introduction

Conclusions

References

Tables

Figures

◀

▶

◀

▶

Back

Close

Full Screen / Esc

Printer-friendly Version

Interactive Discussion



Macro-roughness model of bedrock-alluvial river morphodynamics

L. Zhang et al.

Title Page

Abstract

Introduction

Conclusions

References

Tables

Figures

◀

▶

◀

▶

Back

Close

Full Screen / Esc

Printer-friendly Version

Interactive Discussion



level is maintained, and I_f denotes a flood intermittency factor to account for the fact that only relatively rare flow events are likely to drive incision (Chatanantavet and Parker, 2009). Also I_f is assumed to be a prescribed constant; a more generalized formulation for flow hydrograph is given in Sklar and Dietrich (2006) and DiBiase and Whipple (2011). In interpreting Eq. (6), it should be noted that ν denotes a rock uplift rate for the case of constant base level, or equivalently a rate of base level fall for rock undergoing neither uplift nor subsidence. Below we use the term “rock uplift” as shorthand for the relative vertical velocity between the rock and the point of base level maintenance.

2.3 Character of the CSA model: upstream waves of incision

The MRSAA model (introduced below) has several new features as compared to CSA. These are best illustrated by first characterizing the mathematical nature of CSA in the context of Eq. (6). Let

$$S_b = -\frac{\partial \eta_b}{\partial x} \quad (7)$$

denote the streamwise bedrock surface slope. Reducing Eq. (6) with Eq. (7) the CSA model of Eq. (6) reveals itself as a nonlinear kinematic wave equation with a source term:

$$\frac{\partial \eta_b}{\partial t} - c_b \frac{\partial \eta_b}{\partial x} = \nu \quad (8a)$$

$$c_b = \frac{I_f \beta q_{bc} \rho_c (1 - \rho_c)}{S_b} \quad (8b)$$

Here c_b denotes the wave speed associated with bedrock incision. The form of Eq. (8a) dictates that disturbances in bedrock elevation always move upstream. We will see later that these disturbances can take the form of upstream-migrating knick-points (e.g., Chatanantavet and Parker, 2009).

namics and purely alluvial morphodynamics. The form of the model presented here is simplified in terms of the HSR outlined above, including a constant-width channel and a single sediment source upstream.

3 Macro-Roughness-based Saltation-Abrasion-Alluviation (MRSAA) formulation and its implications for channel evolution

3.1 Formulation for alluvial sediment conservation and cover factor

The geomorphic incision law of the MRSAA model is identical to that of CSA, i.e., Eq. (1b). The essential differences are contained in (a) a formulation for the cover factor p_c that differs from Eq. (2), and (b) the inclusion of alluvial morphodynamics in a way that tracks the spatiotemporal evolution of the bedload transport rate, and allows smooth spatiotemporal transitions between the bedrock-alluvial state and the purely alluvial state.

We formulate the problem by considering a conservation equation for the alluvium, appropriately adapted to include below-capacity transport over a non-erodible surface. The first model of this kind is due to Struiksmma (1999), and further progress has been made by Parker et al. (2009), Izumi and Yokokawa (2011), Izumi et al. (2012), Parker et al. (2013), Tanaka and Izumi (2013) and Zhang et al. (2013). A definition diagram for the derivation of this equation is given in Fig. 4. Bedrock elevation fluctuates locally in space, as seen in Fig. 1 for the field and in Fig. 4 in schematized form. This fluctuation is here characterized by a macro-roughness L_{mr} . We begin by specifying the macroscopic location of the bottom of this bedrock surface η_b (averaged over fluctuations) as the “base” of this rough layer, and locating the “top” of the rough layer at $\eta_b + L_{mr}$. The bedrock is completely exposed when $\eta_a = 0$, partially exposed when $0 < \eta_a < L_{mr}$ and completely alluviated when $\eta_a \geq L_{mr}$. (We amend this formulation below.)

Now let z be the elevation above the bedrock “base” as shown in Fig. 4, and λ_p be the porosity of the alluvial deposit, here assumed to be constant. The cover fraction

Macro-roughness model of bedrock-alluvial river morphodynamics

L. Zhang et al.

Title Page

Abstract

Introduction

Conclusions

References

Tables

Figures

◀

▶

◀

▶

Back

Close

Full Screen / Esc

Printer-friendly Version

Interactive Discussion



Macro-roughness model of bedrock-alluvial river morphodynamics

L. Zhang et al.

Title Page

Abstract

Introduction

Conclusions

References

Tables

Figures

◀

▶

◀

▶

Back

Close

Full Screen / Esc

Printer-friendly Version

Interactive Discussion



associated with a given elevation z is denoted as $\tilde{\rho}_c(z)$, a parameter that is taken to be purely geometrical, invariant in time and representative of the statistical structure of the local elevation variation of the bedrock itself (such as that shown in Fig. 1). As illustrated in Fig. 4, the volume of alluvial sediment per unit area between elevations z and $z + \Delta z$ is $(1 - \lambda_p)\tilde{\rho}_c(z)\Delta z$ and the bedload transport rate q_b is estimated as $\rho_c q_{bc}$, where

$$\rho_c = \tilde{\rho}_c|_{z=\eta_a} \quad (13)$$

For the case of sediment of constant density, the Exner equation for mass balance of alluvial sediment can be expressed as

$$(1 - \lambda_p) \frac{\partial}{\partial t} \int_0^{\eta_a} \tilde{\rho}_c dz = -l_f \frac{\partial \rho_c q_{bc}}{\partial x} \quad (14)$$

where the factor l_f accounts for the fact that morphodynamics is active only during floods. Reducing Eq. (14) with Leibnitz's rule,

$$(1 - \lambda_p) \rho_c \frac{\partial \eta_a}{\partial t} = -l_f \frac{\partial \rho_c q_{bc}}{\partial x} \quad (15)$$

Equations (6) and (15) delineate the formulation encompassing both for bedrock-alluvial rivers and alluvial rivers. In order to complete the problem, it is necessary to define a closure model for ρ_c . The local variation of bedrock elevation is captured by the “macro-roughness” L_{mr} of Fig. 4. Here we seek a formulation that averages over a window capturing a statistically relevant sample of this local variation. It is assumed that ρ_c is a specified, monotonically increasing function of $\chi = \eta_a/L_{mr}$, such that $\rho_c = 0$ when $\eta_a/L_{mr} = 0$ and $\rho_c = 1$ when $\eta_a/L_{mr} = 1$, i.e.

$$\rho_c|_{\chi=0} = 0, \quad (16a)$$

$$\rho_c|_{\chi \geq 1} = 1 \quad (16b)$$

The general form of this relation $\rho_c = f_c(\chi)$ is illustrated in Fig. 5. The simplest functional form for $f_c(\chi)$ satisfying Eq. (16a, b) is a linear relation that is analogous to Eq. (2);

$$\rho_c = \begin{cases} \chi, & \chi \leq 1 \\ 1, & \chi > 1 \end{cases}, \quad (17a)$$

$$\chi = \frac{\eta_a}{L_{mr}} \quad (17b)$$

Note that this cover relation is based on the macro-roughness length L_{mr} rather than the capacity transport q_{bc} of Eq. (2). This is the motivation for referring to the new model presented here as the MRSAA (Macro-Roughness-based Saltation-Abrasion-Alluviation) model.

More simplified versions of such a formulation have been previously presented by Parker et al. (2013), Zhang et al. (2013) and Tanaka and Izumi (2013). The present formulation corrects errors in Parker et al. (2013) and Zhang et al. (2013).

3.2 Character of the alluvial part of the MRSAA problem: alluvial diffusion and downstream-migrating waves of alluviation

Taking $\rho_c = f_c(\chi)$, where f_c is an arbitrary function satisfying the conditions Eq. (16a, b), Eq. (15) can be reduced to

$$\frac{\partial \eta_a}{\partial t} + c_a \frac{\partial \eta_a}{\partial x} = -\frac{1}{1-\lambda_p} l_f \frac{\partial q_{bc}}{\partial x} \quad (18)$$

where

$$c_a = \frac{l_f}{1-\lambda_p} \frac{q_{bc}}{L_{mr} \rho_c} f'_c, \quad (19a)$$

$$f'_c = \frac{df_c}{d\chi} \quad (19b)$$

Neglect of the right-hand side of Eq. (18) yields a kinematic wave equation, where c_a is the wave speed of downstream-directed alluviation.

The form of the equation can be further clarified by rewriting it as

$$\frac{\partial \eta_a}{\partial t} + c_a \frac{\partial \eta_a}{\partial x} - \frac{\partial}{\partial x} \left(v_a \frac{\partial \eta_a}{\partial x} \right) = \frac{\partial}{\partial x} \left(v_a \frac{\partial \eta_b}{\partial x} \right) \quad (20)$$

where

$$v_a = \frac{l_f q_{bc}}{(1 - \lambda_p) S}, \quad (21a)$$

$$S = -\frac{\partial \eta}{\partial x} = -\frac{\partial \eta_b}{\partial x} - \frac{\partial \eta_a}{\partial x} \quad (21b)$$

In the above relation, v_a has the physical meaning of a kinematic diffusivity. In general, q_{bc} , q_{bc}/S and thus v_a are nonlinear functions of S . The alluvial problem thus takes the form of a nonlinear advective-diffusive problem with a source term arising from a bedrock term.

3.3 Full MRSAA formulation: alluvial diffusion, upstream-migration waves of incision, downstream-migrating waves of alluviation

The full MRSAA model consists of the kinematic wave equation with a source term Eq. (8a) for the bedrock part, Eqs. (19)–(21) for the alluvial part, and the linkage between the two embodied in the cover relation of Eq. (17). Restating these equations for emphasis, they are

$$\frac{\partial \eta_b}{\partial t} - c_b \frac{\partial \eta_b}{\partial x} = \nu, \quad (22a)$$

$$c_b = \frac{l_f \beta q_{bc} \rho_c (1 - \rho_c)}{\left(-\frac{\partial \eta_b}{\partial x} \right)} \quad (22b)$$

Macro-roughness model of bedrock-alluvial river morphodynamics

L. Zhang et al.

Title Page

Abstract

Introduction

Conclusions

References

Tables

Figures

◀

▶

◀

▶

Back

Close

Full Screen / Esc

Printer-friendly Version

Interactive Discussion



$$\frac{\partial \eta_a}{\partial t} + c_a \frac{\partial \eta_a}{\partial x} - \frac{\partial}{\partial x} \left(v_a \frac{\partial \eta_a}{\partial x} \right) = \frac{\partial}{\partial x} \left(v_a \frac{\partial \eta_b}{\partial x} \right) \quad (23a)$$

$$c_a = \frac{l_f}{1 - \lambda_p} \frac{q_{bc}}{L_{mr} \rho_c} f'_c, \quad (23b)$$

$$f'_c = \frac{d\rho_c}{d(\eta_a/L_{mr})}, \quad (23c)$$

$$v_a = \frac{l_f q_{bc}}{(1 - \lambda_p) \left[-\frac{\partial}{\partial x} (\eta_a + \eta_b) \right]} \quad (23d)$$

$$\rho_c = \begin{cases} \frac{\eta_a}{L_{mr}}, & \frac{\eta_a}{L_{mr}} \leq 1 \\ 1, & \frac{\eta_a}{L_{mr}} > 1 \end{cases} \quad (24)$$

10 In this way, upstream-migrating incisional waves are combined with downstream-migrating alluvial waves and alluvial diffusion. The relation for cover factor ρ_c is amended, however, in Sect. 3.3.

In MRSAA, then, the spatiotemporal variation of the cover fraction $\rho_c(x, t)$ is specifically tied to the corresponding variation in η_a through Eq. (24). This variation then affects incision through Eq. (22). Consider the wave of alluvium illustrated in Fig. 3. There is no incision ahead of the wave because $\rho_c = 0$. At the peak of the wave, $\eta_a > L_{mr}$, so $\rho_c = 1$ and again there is no incision. Incision can only occur on the rising and falling parts of the wave, where $0 < \rho_c < 1$. It can thus be expected that the spatiotemporal variation in cover thickness η_a will affect the evolution of the long profile of an incising river which undergoes transitions between alluvial and mixed bedrock-alluvial states.

3.4 Amendment of flow model for MRSAA model

The flow model, and in particular Eqs. (9a) and (11), must be modified to include the alluvial formulation, so that S_b is replaced with S , where

$$S = -\frac{\partial \eta}{\partial x} = S_b + S_a, \quad (25a)$$

Macro-roughness model of bedrock-alluvial river morphodynamics

L. Zhang et al.

Title Page

Abstract

Introduction

Conclusions

References

Tables

Figures

◀

▶

◀

▶

Back

Close

Full Screen / Esc

Printer-friendly Version

Interactive Discussion



$$S_b = -\frac{\partial \eta_b}{\partial x}, \quad (25b)$$

$$S_a = -\frac{\partial \eta_a}{\partial x} \quad (25c)$$

Thus Eqs. (9a) and (11a, b) are amended to

$$5 \quad \tau_b = \rho g H S \quad (26)$$

$$H = \left(\frac{Q_f^2}{C Z^2 g B^2 S} \right)^{1/3}, \quad (27a)$$

$$10 \quad \tau^* = \left(\frac{Q_f^2}{C Z^2 g B^2} \right)^{1/3} \frac{S^{2/3}}{R D} \quad (27b)$$

The purely alluvial case, i.e., $p_c = 1$, $f'_c = 0$ and $\eta_b = \text{const} < \eta_a$, results in the purely diffusional relation

$$\frac{\partial \eta_a}{\partial t} = \frac{\partial}{\partial x} \left(v_a \frac{\partial \eta_a}{\partial x} \right) \quad (28)$$

15 in which the diffusivity v_a is a function of $S_a = -\partial \eta_a / \partial x$.

In MRSAA, then, the spatiotemporal variation of the cover fraction $p_c(x, t)$ is specifically tied to the corresponding variation in η_a through Eq. (24). This variation then affects incision through Eq. (22). Consider the wave of alluvium illustrated in Fig. 3. There is no incision ahead of the wave because $p_c = 0$. At the peak of the wave, $\eta_a > L_{mr}$, so
 20 $p_c = 1$ and again there is no incision. Incision can only occur on the rising and falling parts of the wave, where $0 < p_c < 1$. It can thus be expected that the spatiotemporal variation in cover thickness η_a will affect the evolution of the long profile of an incising river which undergoes transitions between alluvial and mixed bedrock-alluvial states.

**Macro-roughness
model of
bedrock-alluvial river
morphodynamics**

L. Zhang et al.

Title Page

Abstract

Introduction

Conclusions

References

Tables

Figures

◀

▶

◀

▶

Back

Close

Full Screen / Esc

Printer-friendly Version

Interactive Discussion



Macro-roughness model of bedrock-alluvial river morphodynamics

L. Zhang et al.

Title Page	
Abstract	Introduction
Conclusions	References
Tables	Figures
◀	▶
◀	▶
Back	Close
Full Screen / Esc	
Printer-friendly Version	
Interactive Discussion	

With this in mind, the “bottom” and “top” of the bedrock, as well as the macro-roughness L_{mr} , should be defined in a statistical sense. This can be done using moments or exceedance probabilities; here we use the latter. Let $p_{c,r}$ denote some low reference cover value (e.g., $p_{c,r} = 0.05$, or 5% cover), $p_{c,1-r}$ represents a corresponding high reference cover (where e.g., $p_{c,1-r} = 1 - p_{c,r} = 0.95$, or 95% cover), and z'_r and z'_{1-r} denote the corresponding bed elevations. An effective “base” of the bedrock, where $\eta_a = 0$, can be located at z'_r , macro-roughness height L_{mr} can be specified as

$$L_{mr} = z'_{1-r} - z'_r \tag{30}$$

and an effective “top” of the bedrock can be specified as $\eta_a + L_{mr}$. This formulation ensures that $p_c = p_{c,r} > 0$ when $\eta_a = 0$.

An appropriately modified form for the cover function is

$$p_c = p_{c,r} + (p_{c,1-r} - p_{c,r})f_c(\chi) \tag{31}$$

where f_c must satisfy the general conditions

$$f_c(0) = 0, \tag{32a}$$

$$f_c(1) = 1, \tag{32b}$$

$$f_c(\infty) = \frac{1 - p_{c,r}}{p_{c,1-r} - p_{c,r}} \tag{32c}$$

and

$$0 < f'_c(0) < \infty \tag{32d}$$

From Eqs. (23a), (31) and (32d), the wave speed at $\eta_a = 0$ is now given as

$$c_a|_{\eta_a=0} = \frac{1}{1 - \lambda_p} \frac{l_f q_{bc}}{L_{ma} p_{c,r}} f'_c(0) < \infty \tag{33}$$



The simplest form satisfying these conditions is given below, and illustrated in Fig. 7:

$$f_c = \begin{cases} \chi & \text{for } 0 \leq \chi \leq \frac{1-p_{c,r}}{p_{c,1-r}-p_{c,r}} \\ \frac{1-p_{c,r}}{p_{c,1-r}-p_{c,r}} & \text{for } \chi > \frac{1-p_{c,r}}{p_{c,1-r}-p_{c,r}} \end{cases} \quad (34)$$

The above relation is used in implementations of the MRSAA below.

5 4 The below-capacity steady-state case common to CSA and MRSAA

The steady-state form of Eq. (6) under below-capacity conditions ($p_c < 1$) can be expressed with the aid of Eq. (2) in the form

$$p_{cs} = 1 - \Lambda, \quad (35a)$$

$$\Lambda = \frac{v}{l_f \beta_s q_{bf}}, \quad (35b)$$

$$10 \quad q_{bcs} = \frac{q_{bf}}{p_{cs}} \quad (35c)$$

where p_{cs} , β_s and q_{bcs} denote steady-state values of p_c , β and q_{bc} , respectively. Equation (35a–c) describe a balance between the incision rate and relative vertical rock velocity (e.g., constant rock uplift rate at constant base level or constant rock elevation with constant rate of base level fall). CSA and MRSAA yield the same solution for this case, which must be characterized before showing how the models differ.

Equation (35a) has an interesting character. When the value of Λ exceeds unity, p_c falls below zero and no steady state solution exists. Equation (35b) reveals that Λ can be interpreted as a dimensionless rock uplift rate. Thus when the rock uplift rate is sufficiently large for Λ to exceed unity, incision cannot keep pace with rock uplift, leading to the formation of a hanging valley. This issue was earlier discussed in Crosby et al. (2007).

Macro-roughness model of bedrock-alluvial river morphodynamics

L. Zhang et al.

Title Page

Abstract

Introduction

Conclusions

References

Tables

Figures

◀

▶

◀

▶

Back

Close

Full Screen / Esc

Printer-friendly Version

Interactive Discussion



In solving for this steady state, and in subsequent calculations, we use the bedload transport relation of Wong and Parker (2006a) rather than the very similar formulation of Fernandez Luque and van Beek (1976); in the case of the former, $\alpha_b = 4$, $n_b = 1.5$ and $\tau_c^* = 0.0495$. We consider two cases: one for which $\beta_s = \beta$ is a specified constant, and one for which only a reference value β_r is specified, and β_s is computed from Eq. (5d).

In the case of a specified constant β , specification of ν , l_f and q_{bf} allow computation of Λ , ρ_{cs} and q_{bcs} from Eq. (35a–c). Further specification of R (here chosen to be 1.65, the standard value for quartz) and D allows the steady-state Shields number τ_s^* to be computed from Eq. (5c). Steady-state bedrock slope S_{bs} can then be computed from Eq. (11b) upon specification of flood discharge Q_f , Chézy resistance coefficient Cz and channel width B . In the case of β_s calculated according to Eq. (7) using a specified reference value β_r , the problem can again be solved with Eqs. (35), (5c) and (11b), but the solution is implicit.

We performed calculations for conditions loosely based on: (a) field estimates for a reach of the bedrock Shimanto River near Tokawa, Japan (Fig. 1), for which bed slope S is about 0.002 and channel width is about 100 m; (b) estimates using relations in Parker et al. (2007) for alluvial gravel-bed rivers with similar slopes, and reasonable choices for otherwise poorly-constrained parameters. The input parameters, $Cz = 10$, $Q_f = 300 \text{ m}^3 \text{ s}^{-1}$, $B = 100 \text{ m}$, are loosely justified in terms of bankfull characteristics of alluvial gravel-bed rivers of the same slope (Parker et al.; 2007; Wilkerson et al.; 2011) as shown in Figs. 8a and b. The value $D = 20 \text{ mm}$ represents a reasonable characteristic size of the substrate (and thus the bedload) for gravel-bed rivers; a typical size for surface pavement is 2 to 3 times this (e.g., Parker et al.; 1982). Intermittency l_f is estimated as 0.05, i.e., 18 days per year, and thus a reasonable estimate for a river subject to frequent heavy storm rainfall. Alluvial porosity is $\lambda_p = 0.35$. Two sediment feed rates were considered. The high feed rate was $3.5 \times 10^5 \text{ tons year}^{-1}$, corresponding to the following steady state parameters at capacity conditions: Shields number $\tau^* = 0.12$, depth $H = 1.5 \text{ m}$, steady state alluvial bed slope $S_e = 0.0026$ and Froude

number $Fr = 0.51$ where

$$Fr = \frac{Q_f}{BH\sqrt{gH}} \quad (36)$$

The low feed rate was 3.5×10^4 tons year⁻¹, corresponding to the following parameters at capacity conditions: Shields number $\tau^* = 0.064$, depth $H = 2.1$ m, steady state alluvial bed slope $S_e = 0.0010$ and Froude number $Fr = 0.32$. The value $\beta_s = 0.05$ km⁻¹ was used for the case of constant abrasion coefficient. This corresponds to a value of α_d of 0.017 km⁻¹, which falls in the middle of the range measured by Kodama (1994) for chert, quartz and andesite (see Fig. 3-41 of Parker, 2008). For the case of variable abrasion coefficient, Eq. (1a) was used with β_r set to 0.05 km⁻¹ and τ_r^* set to 0.12 , i.e., the value for the high feed rate. This value of τ_r^* is about 2.5 times the threshold value of Wong and Parker (2006a).

For the high feed, predicted relations for β_s vs. ν are shown in Fig. 9a; the corresponding predictions for S_{bs} vs. ν are shown in Fig. 9b; the corresponding prediction for ρ_{cs} is shown in Fig. 9c. Both the cases of constant and variable β_s are shown. There are five notable aspects of these figures. (1) In Fig. 9a, the predictions for variable β_s are very similar to the case of constant, specified β_s , and indeed are nearly identical for $\nu \leq 3.3$ mm year⁻¹ (corresponding to $\Lambda \leq 0.05$ in Fig. 9c). (2) In Fig. 9b and c, the predictions for S_{bs} , ρ_{cs} and Λ for variable β_s are again nearly identical to those for constant β_s , and again essentially independent of ν for $\nu \leq 3.3$ mm year⁻¹. (3) In Fig. 9c, ρ_{cs} is only slightly below unity (i.e., ≥ 0.95), and $\Lambda \leq 0.05$ for $\nu \leq 3.3$ mm year⁻¹. (4) For $\nu > 3.3$ mm year⁻¹, the predictions for S_{bs} , ρ_{cs} become dependent on ν , such that S_{bs} increases, and ρ_{cs} decreases, with increasing ν . The values for constant β_s diverge from those for variable β_s , but are nevertheless close to each other up to some limiting value. (5) This limiting value corresponds to $\Lambda = 1$ and thus $\rho_{cs} = 0$ from Eq. (35a); larger values of Λ lead to hanging valley formation. Here $\Lambda = 1$ for the very high values $\nu = 65$ mm year⁻¹ for constant β_s and $\nu = 30$ mm for variable β_s .

**Macro-roughness
model of
bedrock-alluvial river
morphodynamics**

L. Zhang et al.

Title Page

Abstract

Introduction

Conclusions

References

Tables

Figures

◀

▶

◀

▶

Back

Close

Full Screen / Esc

Printer-friendly Version

Interactive Discussion



Macro-roughness model of bedrock-alluvial river morphodynamics

L. Zhang et al.

Title Page

Abstract

Introduction

Conclusions

References

Tables

Figures

◀

▶

◀

▶

Back

Close

Full Screen / Esc

Printer-friendly Version

Interactive Discussion



These results require interpretation. It is seen from Eq. (35a–c) that when $\nu/(l_f\beta_s q_{bf}) = \Lambda \ll 1$, p_c becomes nearly equal to unity (very little exposed bedrock), in which case q_{bf} is constrained to be only slightly smaller than q_{bc} . From Eqs. (5c) and (11), then, S_{bs} is only slightly above the steady state alluvial bed slope S_e . Note that the steady-state bedrock slope decouples from rock uplift rate under these conditions: the predictions for $\nu = 0.2 \text{ mm year}^{-1}$ are nearly identical to this for $\nu = 3.3 \text{ mm year}^{-1}$. This behavior is a specific consequence of the condition $\Lambda \ll 1$ corresponding to a low ratio of uplift rate to a reference incision rate $E_{ref} = l_f\beta_s q_{bf}$. They imply a wide range of conditions for which (a) very little bedrock is exposed, and (b) bedrock slope is independent of uplift rate.

The results for the low feed rate are very similar. The values for variable β_s differ from the constant value β_s in Fig. 10a, but this is because the constant value $\beta_s = 0.05$ was set based on the high feed rate. The results in Fig. 10b and c are qualitatively the same for Fig. 9b and c; the uplift rate below which $\Lambda < 0.05$ is $0.33 \text{ mm year}^{-1}$ for the case of constant β_s , and $0.73 \text{ mm year}^{-1}$ for the case of variable β_s . The critical value of ν beyond which a hanging valley forms is 6.8 mm year^{-1} for constant β_s and 7.1 mm year^{-1} for variable β_s .

The lack of dependence of steady-state bedrock slope S_{bs} on rock uplift rate ν below a threshold value for the steady-state solutions of the CSA model (and thus the MR-SAA model as well) is in stark contrast to earlier work for which the incision rate E_s is assumed to have the following dependence on slope S_b and drainage area A (Slope–Area formulation, Howard and Kerby, 1983):

$$E_s = K S_b^n A^m \quad (37)$$

where A denotes drainage area, n and m are specified exponents, and K is a constant assumed to increase with increasing rock hardness.

In order to compare the steady-state predictions of the Slope–Area relation of Eq. (37) for constant ν with CSA, drainage area A must be taken to be a constant value A_0 so as to correspond to the HSR configuration used here. The steady-state

slope S_{bs} corresponding to a balance between incision and rock uplift is found from Eq. (37) to be

$$S_{bs} = \frac{\nu^{\frac{1}{n}}}{K^{\frac{1}{n}} A_o^{\frac{m}{n}}} \quad (38)$$

5 In their Table 1, Whipple and Tucker (2000) quote a range of values of n , but their most quoted value is 2. We compare the results for CSA for S_{bs} with the predictions from Eq. (38) with $n = 2$ by normalizing against a reference value S_{bsr} corresponding to a reference rock uplift rate ν_r of 0.2 mm year^{-1} . Equation (38) yields

$$\frac{S_{bs}}{S_{bsr}} = \left(\frac{\nu}{\nu_r} \right)^{1/2} \quad (39)$$

10 In Fig. 11, Eq. (39) is compared against the CSA predictions of Figs. 9b and 10b (high and low feed rate, respectively), for both constant and variable β_s . In order to keep the plot within a realistic range, only values of ν between 0.2 mm year^{-1} and 10 mm year^{-1} (the upper limit corresponding to Dadson et al., 2003), have been used in the CSA results. The remarkable insensitivity of the CSA predictions for steady-state slope S_{bs} on rock uplift rate is readily apparent from the figure.

20 One more difference between the CSA and Slope–Area formulations is worth noting. If the Slope–Area relation is installed into Eq. (6) in place of CSA, it is readily shown that bedrock slope gradually relaxes to zero in the absence of rock uplift. CSA does not obey the same behavior under the constraint of constant sediment feed rate: Figs. 9b and 10b indicate that bedrock slope converges to a constant, nonzero value as rock uplift declines to zero. This is not necessarily a shortcoming of CSA; the sediment feed rate can be expected to decline as relief declines.

Macro-roughness model of bedrock-alluvial river morphodynamics

L. Zhang et al.

Title Page	
Abstract	Introduction
Conclusions	References
Tables	Figures
◀	▶
◀	▶
Back	Close
Full Screen / Esc	
Printer-friendly Version	
Interactive Discussion	



5 Boundary conditions and parameters for numerical calculations with MRSAA model

Having conducted a fairly thorough analysis of the steady state common to the CSA and MRSAA models, it is now appropriate to move on to examples of behavior that can be captured by the MRSAA model but not the CSA model. Before doing so, however, it is necessary to delineate the boundary conditions and other assumptions used in the MRSAA model.

Let L denote the length of the reach. Equation (22a) indicates that the formulation for bedrock incision is first-order in x and so requires only one boundary condition. The example considered here is that of a downstream bedrock elevation, i.e., base level, that is set to 0:

$$\eta_b|_{x=L} = 0 \quad (40)$$

According to Eq. (15), or alternatively Eq. (23a), the alluvial formulation is second-order in x and thus requires two boundary conditions. The following boundary condition applies at the upstream end of the reach; where $q_{bf}(t)$ denotes a feed rate which may vary in time,

$$q_b|_{x=0} = q_{bf}(t) \quad (41)$$

At the downstream end, a free boundary condition is applied for $\eta_a/L_{mr} < 1$, and a fixed boundary condition is applied for $\eta_a/L_{mr} \geq 1$ as follows:

$$\left[p_c(1 - \lambda_p) \frac{\partial \eta_a}{\partial t} + I_f \frac{\partial p_c q_{bc}}{\partial x} \right] \Big|_{x=L} = 0 \quad \text{if} \quad \left[\frac{\eta_a}{L_{mr}} \right] \Big|_{x=L} < 1 \quad (42a)$$

$$\eta_a|_{x=L} = L_{mr} \quad \text{if} \quad \left[\frac{\eta_a}{L_{mr}} \right] \Big|_{x=L} \geq 1 \quad (42b)$$

Here Eq. (42a) specifies a free boundary in the case of partial alluviation, so allowing below-capacity sediment waves to exit the reach. Equation (42b), on the other hand, fixes the maximum downstream elevation at $\eta = \eta_a = L_{mr}$.

Macro-roughness model of bedrock-alluvial river morphodynamics

L. Zhang et al.

Title Page

Abstract

Introduction

Conclusions

References

Tables

Figures

◀

▶

◀

▶

Back

Close

Full Screen / Esc

Printer-friendly Version

Interactive Discussion



Macro-roughness model of bedrock-alluvial river morphodynamics

L. Zhang et al.

[Title Page](#)
[Abstract](#)
[Introduction](#)
[Conclusions](#)
[References](#)
[Tables](#)
[Figures](#)




[Back](#)
[Close](#)
[Full Screen / Esc](#)
[Printer-friendly Version](#)
[Interactive Discussion](#)


In order to illustrate the essential features of the new formulation of the MRSAA model for morphodynamics of mixed bedrock-alluvial rivers, it is useful to consider the most simplified case that illustrates its expanded capabilities compared to the CSA model. Here we implement the HSR simplification. In addition, based on the results of the previous section, we approximate β_s as a prescribed constant. Finally, we assume that the clasts of the abrading bedload are sufficiently hard compared to the bedrock so that grain size D can be approximated as a constant. These constraints are easily relaxed.

6 Sediment waves over a fixed bed: stripping and emplacement of alluvial layer and advection–diffusion of a sediment pulse

Here three numerical cases using the MRSAA model are studied: (1) stripping of an alluvial cover to bare bed; (2) emplacement of an alluvial cover over a bare bed; and (3) advection–diffusion of an alluvial pulse over a bare bed. Reach length L is 20 km. As the time for alluvial response is short compared to incisional response, β_s and ν are set equal to zero for these calculations. In addition, flood intermittency I_f is set to unity so as to illustrate the migration from feed point to the end of the reach under the condition of continuous flow. The macro-roughness L_{mr} is set to 1 m based on visual observation of the Shimanto River near Tokawa, Japan. The values for Cz , Q_f , B , D and λ_p are the same as in Sect. 5, i.e., $Cz = 10$, $Q_f = 300 \text{ m}^3 \text{ s}^{-1}$, $B = 100 \text{ m}$, $D = 20 \text{ mm}$ and $\lambda_p = 0.35$. Bedrock slope S_b , which is constant due to the absence of abrasion, is set to 0.004. The above numbers combined with Eqs. (5c) (using the constants of the formulation of Wong and Parker, 2006a), Eq. (27a) and (27b) yield the following values: depth $H = 1.32 \text{ m}$, Froude number $Fr = 0.63$, Shields number $\tau^* = 0.016$ and capacity bedload transport rate $q_{bc} = 0.0017 \text{ m}^2 \text{ s}^{-1}$.

None of these three cases can be treated using CSA. They thus illustrate capabilities unique to MRSAA.

6.1 Alluvial stripping

The case of stripping of an initial alluvial layer to bare bedrock is considered here. In this simulation, the bedload feed rate $q_{bf} = 0$ and the initial thickness of alluvial cover η_a is set to 0.8 m, i.e., 80 % of the macro-roughness length L_{mr} . To drive stripping of the alluvial layer, the feed rate is set equal to zero. Figure 12a shows how the alluvial cover is progressively stripped off from upstream to downstream as a wave of alluvial rarification migrates downstream. The alluvial layer is completely removed after a little more than 0.12 years.

Of interest in Fig. 12a is the fact that the wave of stripping maintains constant form in spite of the fact that the diffusive term in Eq. (23a) should cause the wave to spread. The reason the wave does not spread is the nonlinearity of the wave speed c_a in Eq. (23b); since ρ_c enters into the denominator of the right-hand side of the equation, wave speed is seen to increase as ρ_c decreases, and thus as η_a decreases. As a result, the lower portion of the wave tends to migrate faster than the higher portion, so sharpening the wave and opposing diffusion.

6.2 Emplacement of an alluvial layer over an initially bare bed

In this simulation, the initial thickness of alluvium η_a is set to zero and the sediment feed rate is set to $0.0013 \text{ m}^2 \text{ s}^{-1}$, i.e., 80 % of the capacity value. The result of the calculation is shown in Fig. 12b. Here nonlinear advection and diffusion act in concert to cause the wave of alluviation to spread. The steady-state thickness of alluvium is 0.83 m; by 0.1 years it has been emplaced only down to about 5 km from the source.

6.3 Propagation of a pulse of alluvium over an initially bare bed

In this example the initial bed is bare of sediment. The sediment feed rate is set equal to $0.0012 \text{ m}^2 \text{ s}^{-1}$, i.e., 70 % of the capacity value for 0.05 years from the start of the run, and then dropped to zero for the rest of the run. Figure 12c shows the propagation of

Macro-roughness model of bedrock-alluvial river morphodynamics

L. Zhang et al.

Title Page

Abstract

Introduction

Conclusions

References

Tables

Figures

◀

▶

◀

▶

Back

Close

Full Screen / Esc

Printer-friendly Version

Interactive Discussion



a damped alluvial pulse through the reach, with complete evacuation of the pulse in a little more than 0.15 years. Nonlinear advection acts against diffusion to suppress the spreading of the upstream side of the pulse, but advection acts together with diffusion to drive spreading of the downstream side of the pulse.

7 Comparison of evolution to steady state with both rock uplift and incision using CSA and MRSAA

Here we consider three cases of channel profile evolution to steady state that include both rock uplift and incision. In the first case, the initial bedrock slope is set to a value below the steady state value, and the sediment feed rate is set to a value that is well above the steady state value for the initial bedrock slope, causing early-stage massive alluviation. The configuration for the second case is a simplified version of a graben with a horst upstream and a horst downstream. The configuration for the third case is such that there is an alluviated river mouth downstream and a bedrock-alluvial transition upstream. In all cases, MRSAA predicts evolution that cannot be predicted by CSA.

7.1 Evolution of bedrock profile with early-stage massive alluviation

Here we set Q_f , B , Cz , D and λ_p to the same values as Sect. 6. The reach length L is 20 km, the flood intermittency I_f is set to 0.05, macro-roughness L_{mr} is set to 1 m, initial alluvial thickness $\eta_a|_{t=0} = 0.5$ m, downstream bed elevation $\eta_b|_{x=L} = 0$ and the abrasion coefficient β_s is 0.05 km^{-1} . The initial bed slope is 0.004. The feed rate is set to twice the capacity rate for this slope, i.e., $q_{bf} = 0.0033 \text{ m}^2 \text{ s}^{-1}$. The uplift rate is set to 5 mm year^{-1} . It should be noted, however, than in analogy Fig. 10b, the steady-state bedrock slope for this feed rate is independent of the uplift rate for $v \leq 5 \text{ m year}^{-1}$. This is because the steady-state value of Λ is 0.019, i.e., $\ll 1$.

The results for the CSA model are shown in Fig. 13a. The bed slope evolves from the initial value of 0.004 to a final steady-state value of 0.0068. Evolution is achieved solely

Macro-roughness model of bedrock-alluvial river morphodynamics

L. Zhang et al.

Title Page

Abstract

Introduction

Conclusions

References

Tables

Figures

◀

▶

◀

▶

Back

Close

Full Screen / Esc

Printer-friendly Version

Interactive Discussion



7.3 Evolution of river profile with an alluviated zone corresponding to a river mouth at the downstream end

In this example Cz , Q_f , B , D , λ_p , β_s , L_{mr} , L and $\eta_{a|t=0}$ are again set to the values chosen in Sect. 7.1. The bedload feed rate is $0.00083 \text{ m}^2/\text{s}$; the steady-state bedrock slope S_b associated with this feed rate is 0.0026 for $v < 5 \text{ mm year}^{-1}$ (Fig. 10b). The initial bedrock slope is set, however, to the higher value 0.004 . The rock uplift rate v for this case is set to 0 , for which the steady-state slope is again 0.0026 .

The result of CSA for this case with base level $\eta_b|_{x=L}$ maintained at 0 is shown in Fig. 15. As in the case of Sect. 7.1, the bedrock slope evolves from the initial value of 0.004 to the steady-state value 0.0026 by means of an upstream-migrating knickpoint. Only 4000 years of evolution are shown in the figure, by which time the knickpoint is 4.8 km from the feed point.

MRSAA is implemented with somewhat different initial and downstream boundary conditions, in order to model the case of bed that remains alluviated at the downstream end. This condition thus corresponds to an alluviated river mouth. The initial bedrock slope is again 0.004 , and the downstream bedrock elevation $\eta_b|_{x=L}$ is again 0 m . Downstream alluvial elevation $\eta_a|_{x=L}$, however, is held at 10 m , so that the downstream end is completely alluviated. The initial slope S for the top of the bed is 0.0021 , a value chosen so that the bed elevation equals the bedrock elevation at the upstream end.

Results of the MRSAA simulation are shown in Fig. 16a–f. Figure 16a–c shows the early-stage evolution, i.e., at $t = 0$, 10 and 100 years. Over this period, a bedrock-alluvial transition (from mixed bedrock-alluvial to purely alluvial) migrates downstream from the feed point to $x = 13.6 \text{ km}$, i.e., 6.4 km upstream of the downstream end of the domain. Bedrock incision is negligible over this period.

Figure 13d–f show the bedrock and top bed profiles for 1000 , 2000 and 4000 years. Over this period, the bedrock-alluvial transition migrates upstream. As it does so, the bedrock slope downstream of $x = 13.6 \text{ km}$ remains alluviated and does not change.

Macro-roughness model of bedrock-alluvial river morphodynamics

L. Zhang et al.

Title Page

Abstract

Introduction

Conclusions

References

Tables

Figures

◀

▶

◀

▶

Back

Close

Full Screen / Esc

Printer-friendly Version

Interactive Discussion



$$\alpha_d = \frac{1}{3}\beta_c \quad (\text{A4b})$$

Equation (A4a) is the differential form of Sternberg's Law; α_d is a diminution coefficient with units L^{-1} . The exponential form of Eq. (3) corresponds to the case of spatially constant α_d .

The incision rate of the bedrock E is the rate of volume loss of bedrock per unit area per unit time, times the volume lost per strike, or thus

$$E = \frac{q_b}{V_p L_s} \beta^* V_p (1 - \rho_c) = \beta^* q_b (1 - \rho_c) = \beta q_{bc} \rho_c (1 - \rho_c),$$

$$\beta = \frac{\beta^*}{L_s} \quad (\text{A5})$$

The above relation is identical to Eq. (1b).

Acknowledgements. The participation of Zhang and Fu in this work was made possible by the National Natural Science Foundation of China (Grant Nos. 51379100 and 51039003). The participation of Parker and Stark was made possible in part by a grant from the US National Science Foundation (Grant No. EAR-1124482 for Parker. and Grant Nos. EAR-1148176. EAR-1124114 and CMMI-1331499 for Stark). The participation of Inoue was made possible by support from the Hokkaido Regional Development Bureau.

References

- An, C. G., Fu, X. D., and Parker, G.: River morphological evolution in earthquake-hit region: effects of floods and pulsed sediment supply, in: River Flow 2014 Conference, Lausanne, Switzerland, September 3–5, p. 7, 2014.
- Chatanantavet, P. and Parker, G.: Physically based modeling of bedrock incision by abrasion, plucking, and macroabrasion, *J. Geophys. Res.*, 114, F04018, doi:10.1029/2008JF001044, 2009.

**Macro-roughness
model of
bedrock-alluvial river
morphodynamics**

L. Zhang et al.

Title Page

Abstract

Introduction

Conclusions

References

Tables

Figures

◀

▶

◀

▶

Back

Close

Full Screen / Esc

Printer-friendly Version

Interactive Discussion



Macro-roughness model of bedrock-alluvial river morphodynamics

L. Zhang et al.

Title Page

Abstract

Introduction

Conclusions

References

Tables

Figures

◀

▶

◀

▶

Back

Close

Full Screen / Esc

Printer-friendly Version

Interactive Discussion



- Turowski, J. M.: Stochastic modeling of the cover effect and bedrock erosion, *Water Resour. Res.*, 45, W03422, doi:10.1029/2008WR007262, 2009.
- Turowski, J. M.: Semi-alluvial channels and sediment-flux-driven bedrock erosion, in: *Gravel Bed Rivers: Processes, Tools, Environments*, edited by: Church, M., Biron, P. M., and Roy, A., 1st edn., ch. 29, John Wiley & Sons, 401–416, 2012.
- 5 Turowski, J. M., Lague, D., and Hovius, N.: Cover effect in bedrock abrasion: a new derivation and its implications for the modeling of channel morphology, *J. Geophys. Res.*, 112, F04006, doi:10.1029/2006JF000697, 2007.
- Whipple, K. X.: Bedrock rivers and the geomorphology of active orogens, *Ann. Rev. Earth Planet. Sci.*, 32, 151–185, 2004.
- 10 Whipple, K. X. and G. E. Tucker: Dynamics of the stream-power river incision model: implications for height limits of mountain ranges, landscape response timescales, and research needs, *J. Geophys. Res.*, 104, 17661–17674, 1999.
- Whipple, K. X. and Tucker, G. E.: Implications of sediment-flux-dependent river incision models for landscape evolution, *J. Geophys. Res.*, 107, 2039, doi:10.1029/2000JB000044, 2002.
- 15 Wilcock, P. R. and Crowe, J. C.: Surface-based transport model for mixed-size sediment, *J. Hydraul. Eng.*, 129, 120–128, 2003.
- Wilkerson, G. V. and Parker, G.: Physical basis for quasi-universal relations describing bankfull hydraulic geometry of sand-bed rivers, *J. Hydraul. Eng.*, 137, 739–753, 2011.
- 20 Wong, M. and Parker, G.: Reanalysis and correction of bed-load relation of Meyer-Peter and Müller using their own database, *J. Hydraul. Eng.*, 132, 1159–1168, 2006a.
- Wong, M. and Parker, G.: One-dimensional modeling of bed evolution in a gravel bed river subject to a cycled flood hydrograph, *J. Geophys. Res.*, 111, F3018, doi:10.1029/2006JF000478, 2006b.
- 25 Xu, Q., Fan, X. M., Huang, R. Q., and Van Westin, C.: Landslide dams triggered by the Wenchuan Earthquake, Sichuan Province, south west China, *Bull. Eng. Geol. Environ.*, 68, 373–386, 2009.
- Zhang, L., Fu, X. D., Stark, C. P., Fernandez, R., and Parker, G.: Modeling of incision of bedrock rivers subject to temporally varying sediment supply, *Proceedings of 2013 IAHR World Congress*, Tsinghua University Press, China, 11 p., Chengdu, China, 8–13 September 2013.
- 30

Table A1. Nomenclature.

A	upstream drainage area [L^2]
B	channel width [L]
CSA	acronym for Capacity-based Saltation-Abrasion model
Cz	dimensionless Chézy resistance coefficient [-]
c_a	speed of propagation of an alluvial disturbance (positive downstream) [$L T^{-1}$]
c_b	speed of propagation of an incisional disturbance (positive downstream) [$L T^{-1}$]
D, D_u	characteristic grain size of clasts effective in abrading the bed; upstream value of D [L]
E	bedrock incision rate [$L T^{-1}$]
Fr	Froude number = $Q_i/[BH(gH)^{1/2}]$ [-]
f_c	function of χ describing cover fraction [-]
g	gravitational acceleration [$L T^{-2}$]
H	flow depth [$L T^{-1}$]
HSR	acronym for Highly Simplified Reach
I_f	flood intermittency = fraction of time the river is in flood [-]
k_v	coefficient in Eq. (5a) [-]
L	reach length [L]
L_{half}	distance a clast travels to lose half its size (diameter) by abrasion [L]
L_{mr}	height of macro-roughness height [L]
MRSAA	acronym for Macro-Roughness-based Saltation-Abrasion-Alluviation model
n_b	exponent in bedload transport relation [-]
p_c	areal fraction of bed that is covered by alluvium [-]
p_{cs}	steady-state value of p_c [-]
$p_{c,r}$	lower reference cover fraction (0.05 herein) [-]
$p_{c,1-r}$	upper reference cover fraction (0.95 herein) [-]
Q_f	flood discharge [$L^3 T^{-1}$]
q_b, q_{bc}, q_{bcs}	volume bedload transport rate per unit width; capacity value of q_b ; steady-state value of q_{bc} [$L^2 T^{-1}$]
q_{bf}	feed, or supply value of q_b [$L^2 T^{-1}$]
q_{bk}	value of q_b at knickpoint [$L^2 T^{-1}$]
R	submerged specific gravity of sediment clasts [-]
R_f	= $v_s/(RgD)^{1/2}$ [-]
S, S_b, S_a	bed slope; slope of bedrock; $-\partial\eta_a/\partial x$ [-]
S_{bi}, S_{bs}	initial bedrock slope; steady-state bedrock slope [-]
$S_{b,u}, S_{b,l}$	bedrock slope upstream of a knickpoint; bedrock slope downstream of a knickpoint [-]
S_e	steady state alluvial bed slope at capacity [-]

**Macro-roughness
model of
bedrock-alluvial river
morphodynamics**

L. Zhang et al.

Title Page

Abstract Introduction

Conclusions References

Tables Figures

◀ ▶

◀ ▶

Back Close

Full Screen / Esc

Printer-friendly Version

Interactive Discussion



Macro-roughness model of bedrock-alluvial river morphodynamics

L. Zhang et al.

Table A1. Continued.

T, T_h, T_l	period of cycled hydrograph; duration of high flow; duration of low flow [T]
U	flow velocity during floods [$L T^{-1}$]
x	streamwise distance [L]
\hat{x}	x/L [–]
x_k	distance to knickpoint [L]
t	time [T]
u_*	shear velocity = $(\tau_b/\rho)^{1/2}$ [$L T^{-1}$]
v_s	fall velocity of a clast [$L T^{-1}$]
Y	bedrock modulus of elasticity [M/LT^2]
z, z'	vertical coordinates [L]
z'_c	bed elevation such that cover fraction $\rho_c = \rho_{c,r}$ [L]
z'_{1-r}	bed elevation such that $\rho_c = \rho_{c,1-r}$ [L]
α_b	coefficient in bedload transport relation [–]
α_d	diminution coefficient for an abrading clast [L^{-1}]
β, β_r, β_s	coefficient of wear (abrasion); reference value of β , steady-state value of β [L^{-1}]
χ	$= \eta_a/L_{mr}$ [–]
Γ	$= Q_f^2/(Cz^2gB^2)^{1/3}/(RD)$ [–]
η, η_a, η_b	bed elevation; thickness of alluvial layer; bedrock elevation [L]
Λ	$= \nu/(l_f\beta_s q_{br})$ [–]
λ_b	porosity of alluvial deposit [–]
ν_a	alluvial diffusivity defined in Eq. (21a) [$L^2 T^{-1}$]
ρ	density of water [ML^{-3}]
σ_t	rock tensile strength [$ML^{-1} T^{-2}$]
τ^*, τ_c^*	Shields number = $u_*^2/(RgD)$; critical value of τ^* at threshold of motion [–]
τ_b	bed shear stress [$ML^{-1} T^{-2}$]
ν	relative vertical speed between the (nondeforming) rock underlying the channel and the point at which base level is maintained, e.g., rock uplift rate or base level fall rate [$L T^{-1}$]

Title Page

Abstract

Introduction

Conclusions

References

Tables

Figures

◀

▶

◀

▶

Back

Close

Full Screen / Esc

Printer-friendly Version

Interactive Discussion



**Macro-roughness
model of
bedrock-alluvial river
morphodynamics**L. Zhang et al.

**a)****b)**

Figure 1. Views of the Shimanto River, a mixed alluvial-bedrock river in Shikoku, Japan. **(a)** View of channel. **(b)** View of macroscopic roughness of the bed and alluvial patches. River width is about 100 m.

Title Page

Abstract

Introduction

Conclusions

References

Tables

Figures

◀

▶

◀

▶

Back

Close

Full Screen / Esc

Printer-friendly Version

Interactive Discussion



Macro-roughness model of bedrock-alluvial river morphodynamics

L. Zhang et al.

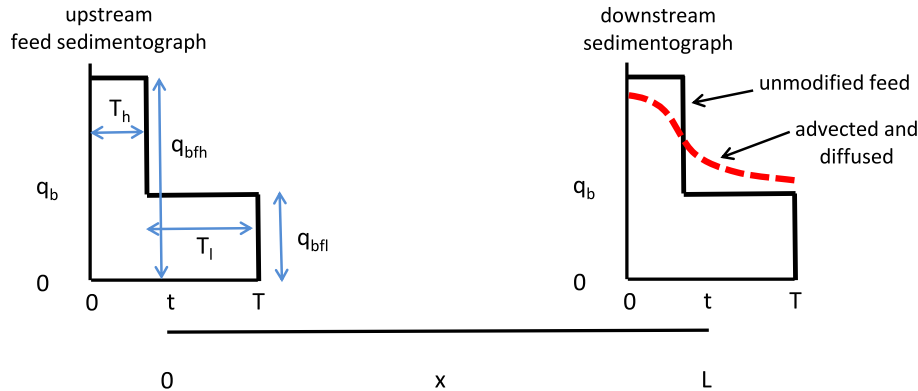


Figure 2. Schematic diagram illustrating downstream modification of a sedimentograph. At the upstream feed point ($x = 0$, left), the bedload transport rate q_b takes the high feed value $q_{bf,h}$ for time T_h and the low feed value $q_{bf,l}$ time T_l , for a total cyclic time $T = T_h + T_l$. At the downstream end ($x = L$, right) (i) the solid line predict the unaltered sedimentograph at the downstream end of the reach, assumed to have propagated instantaneously from the supply point; and (ii) and the dashed line represents the sedimentograph as modified by advective-diffusive effects.

Macro-roughness model of bedrock-alluvial river morphodynamics

L. Zhang et al.

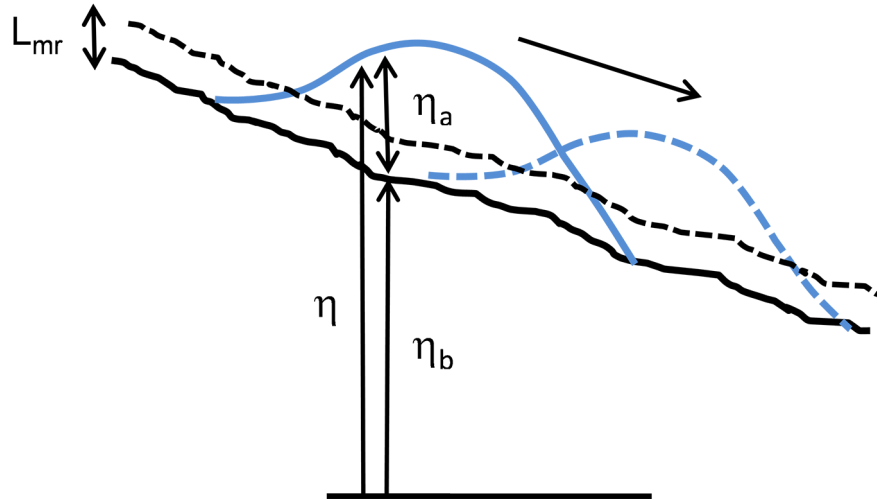


Figure 3. Schematic diagram illustrating the propagation of a wave of sediment over bedrock. Here η_b denotes the elevation of the bottom of the bedrock, L_{mr} denotes the bedrock macro-roughness thickness, η_a denotes the thickness of the alluvial cover (which may be $\ll \eta_b + L_{mr}$) and $\eta = \eta_b + \eta_a$ denotes the elevation of the top of the alluvium.

Title Page

Abstract

Introduction

Conclusions

References

Tables

Figures

◀

▶

◀

▶

Back

Close

Full Screen / Esc

Printer-friendly Version

Interactive Discussion



Macro-roughness model of bedrock-alluvial river morphodynamics

L. Zhang et al.

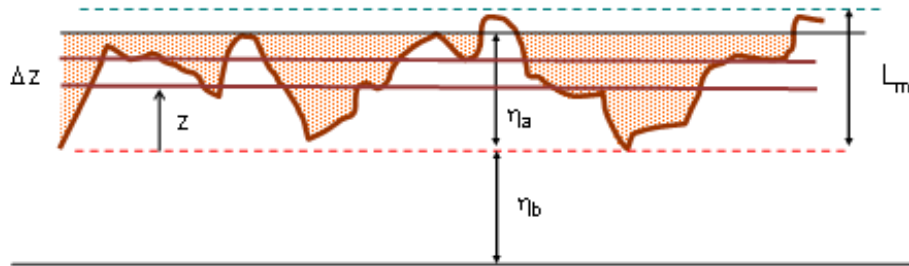


Figure 4. Schematic diagram for derivation of the Exner equation of sediment continuity over a bedrock surface. Here z is the elevation above the bottom of the bedrock layer.

Title Page

Abstract

Introduction

Conclusions

References

Tables

Figures

◀

▶

◀

▶

Back

Close

Full Screen / Esc

Printer-friendly Version

Interactive Discussion



Macro-roughness model of bedrock-alluvial river morphodynamics

L. Zhang et al.

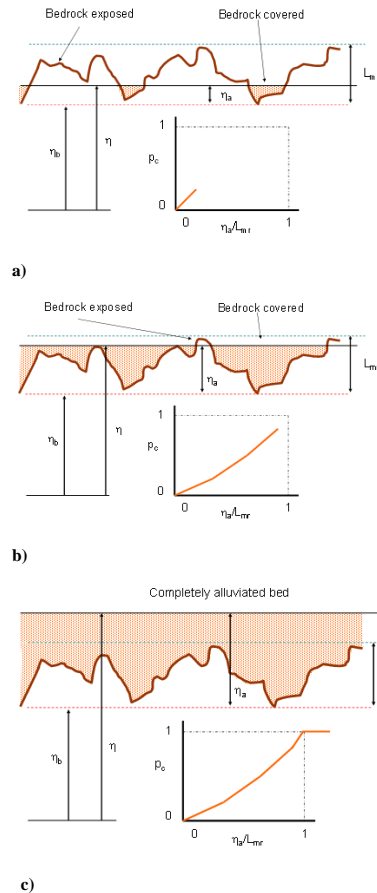


Figure 5. Illustration of the relation between areal fraction of alluvial cover of bedrock p_c and $\chi = \eta_a / L_{mr}$ for MRSAA (Macro-Roughness-based Saltation-Abrasion Alluviation model). **(a)** Low cover. **(b)** Intermediate cover. **(c)** Complete alluviation above the top of the bedrock.

Macro-roughness model of bedrock-alluvial river morphodynamics

L. Zhang et al.

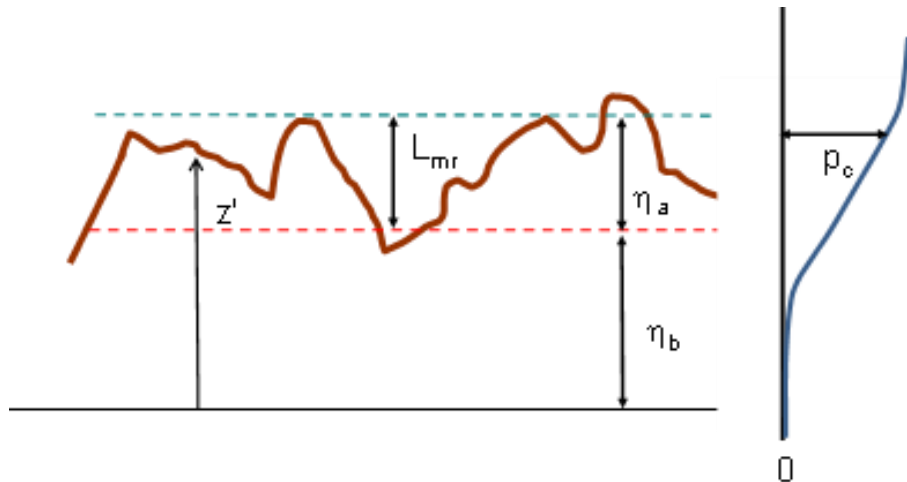


Figure 6. Modification of formulation to account for statistical structure of bedrock roughness. Here z' = elevation above an arbitrary datum, and $p_c(z')$ is now interpreted as the probability that point z' does not correspond to bedrock (i.e., falls within water or alluvium rather than bedrock). The cover factor for alluvial thickness η_a equals $p_c(\eta_a)$. The points η_b and $\eta_b + L_{ma}$ are determined in terms of specified exceedance fractions r and $1 - r$ and $1 = r$ of p_c .

Title Page

Abstract

Introduction

Conclusions

References

Tables

Figures

◀

▶

◀

▶

Back

Close

Full Screen / Esc

Printer-friendly Version

Interactive Discussion



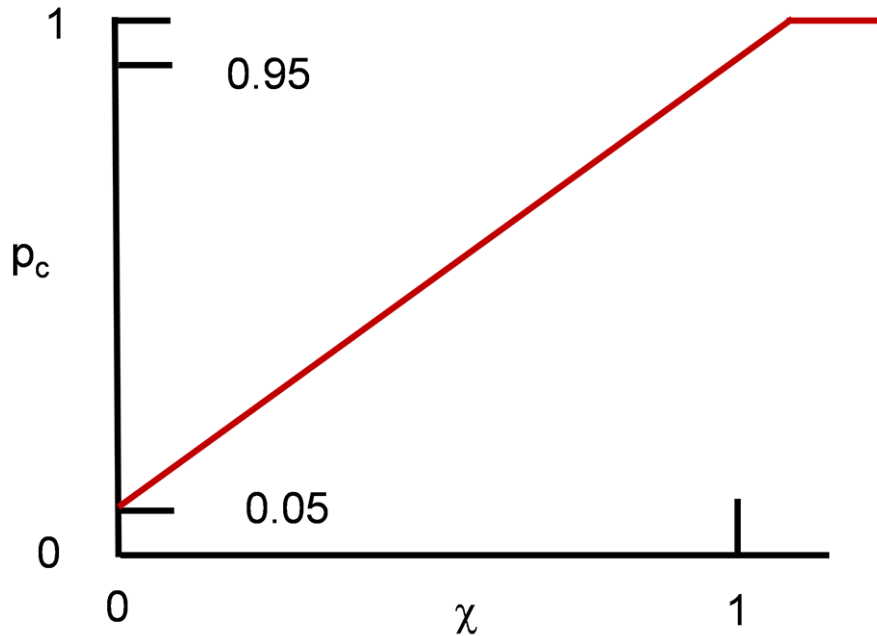


Figure 7. Simplest modified cover function for the MRSAA model satisfying the conditions $p_c(0) = r$, $p_c(1) = 1 - r$ and $p_c(\infty) = 1$, where in this case $r = 0.05$.

Macro-roughness model of bedrock-alluvial river morphodynamics

L. Zhang et al.

Title Page	
Abstract	Introduction
Conclusions	References
Tables	Figures
◀	▶
◀	▶
Back	Close
Full Screen / Esc	
Printer-friendly Version	
Interactive Discussion	



Macro-roughness model of bedrock-alluvial river morphodynamics

L. Zhang et al.

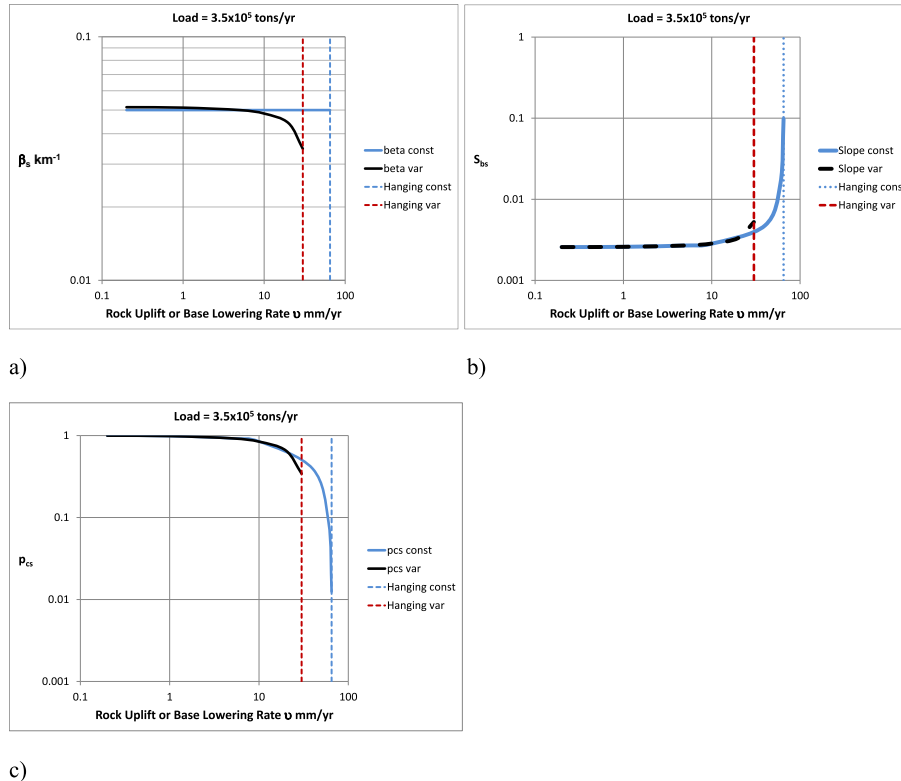


Figure 9. Variation of (a) abrasion coefficient β_s , (b) bedrock slope S_{bs} and (c) cover fraction ρ_{CS} with rock uplift or base lowering rate ν at steady state, with a high bedload feed rate (3.5×10^5 tons year⁻¹). The cases of constant, specified β_s and β_s varying according to Eq. (29) are shown. The vertical lines denote the incipient conditions for the formation of a hanging valley. The predictions are the same for the CSA and MRSAA models.

Title Page

Abstract Introduction

Conclusions References

Tables Figures

◀ ▶

◀ ▶

Back Close

Full Screen / Esc

Printer-friendly Version

Interactive Discussion



Macro-roughness model of bedrock-alluvial river morphodynamics

L. Zhang et al.

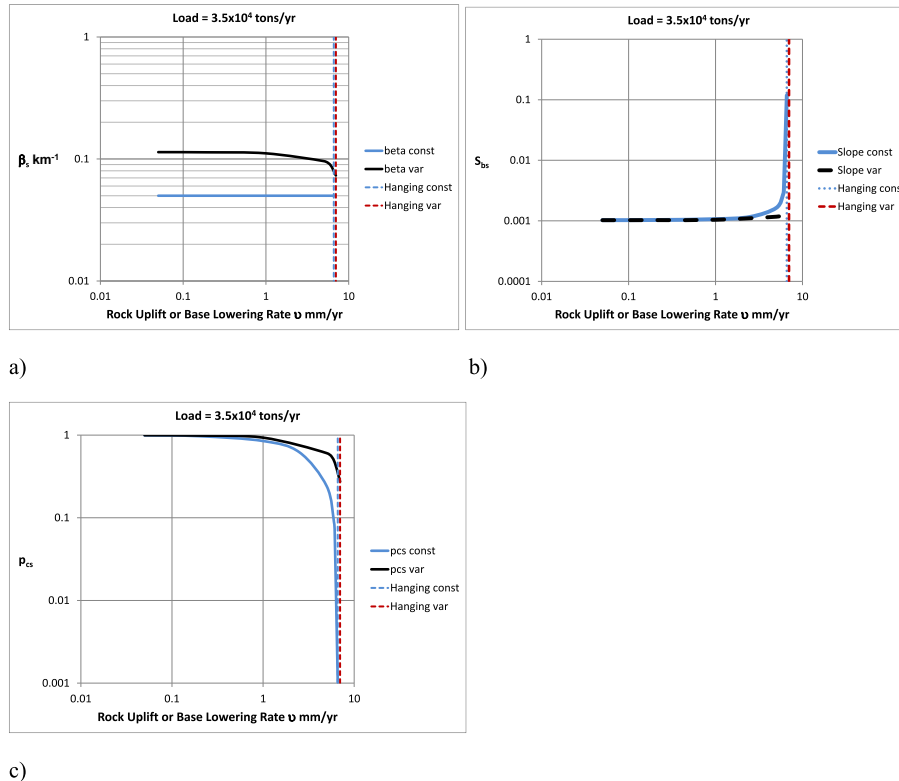


Figure 10. Variation of (a) abrasion coefficient β_s , (b) bedrock slope S_{bs} and (c) cover fraction ρ_{cs} with rock uplift or base lowering rate ν at steady state, with the high bedload feed rate (3.5×10^4 tons year⁻¹). The cases of constant, specified β_s and β_s varying according to Eq. (29) are shown. The vertical lines denote the incipient conditions for the formation of a hanging valley. The predictions are the same for the CSA and MRSAA models.

Title Page

Abstract Introduction

Conclusions References

Tables Figures

◀ ▶

◀ ▶

Back Close

Full Screen / Esc

Printer-friendly Version

Interactive Discussion



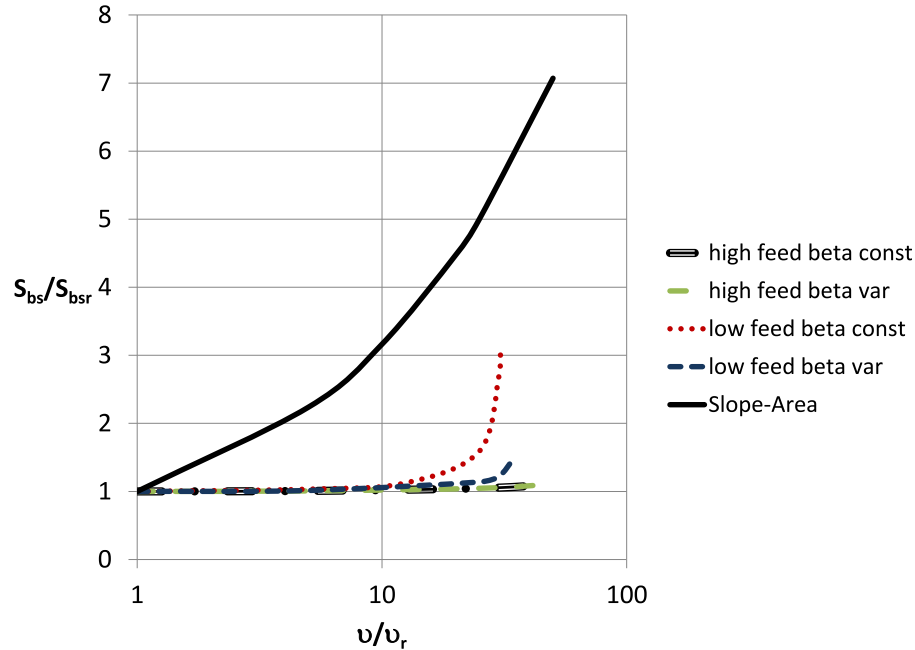


Figure 11. Normalized steady-state bedrock slope vs. normalized rock uplift rate as predicted by the CSA model for a low and a high feed rate, and constant and variable abrasion coefficient. The results are the same for the MRSAA model. Also shown is the prediction of a model for which the incision rate is specified in terms of bedrock slope and upstream drainage area. Note that the predictions for steady-state bedrock slope of the CSA model are insensitive to the rock uplift rate over a wide range.

Macro-roughness model of bedrock-alluvial river morphodynamics

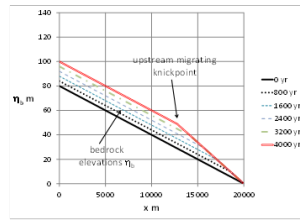
L. Zhang et al.

Title Page	
Abstract	Introduction
Conclusions	References
Tables	Figures
◀	▶
◀	▶
Back	Close
Full Screen / Esc	
Printer-friendly Version	
Interactive Discussion	

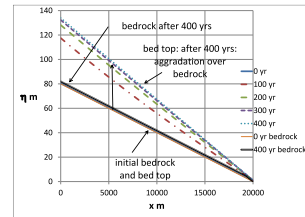


Macro-roughness model of bedrock-alluvial river morphodynamics

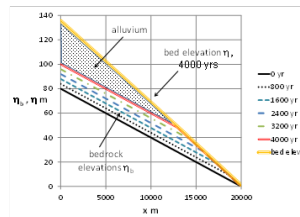
L. Zhang et al.



a)



b)



c)

Figure 13. (a) Progression to steady state after an impulsive increase in sediment supply: CSA model. (b) Progression to steady state after an impulsive increase in sediment supply: MRSAA model, early stage. (c) Progression to steady state after an impulsive increase in sediment supply: MRSAA model, late stage. Note the bedrock knickpoints in (a) and (b), and the migrating alluvial-bedrock transition in (c).

Macro-roughness model of bedrock-alluvial river morphodynamics

L. Zhang et al.

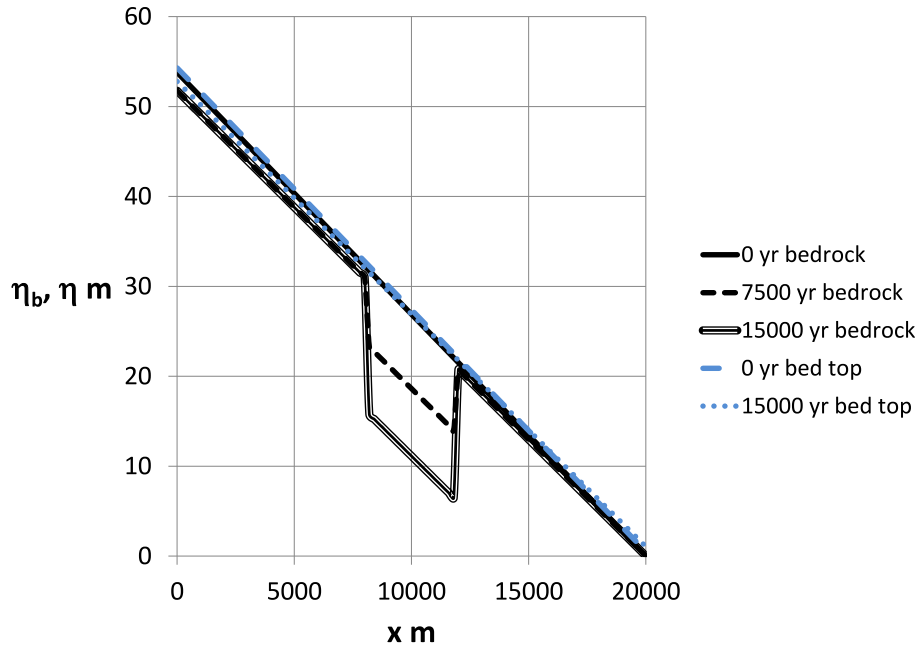


Figure 14. Evolution predicted by the MRSAA model for simplified, 1-D the case of a graben bounded by two horsts. Note the bedrock-alluvial and alluvial-bedrock transitions. By 15 000 years, the bed top has reached steady state, even though the bedrock surface in the graben continues to subside. Horst rock uplift rate and graben rock subsidence rate are assumed constant for simplicity.

Title Page	
Abstract	Introduction
Conclusions	References
Tables	Figures
◀	▶
◀	▶
Back	Close
Full Screen / Esc	
Printer-friendly Version	
Interactive Discussion	



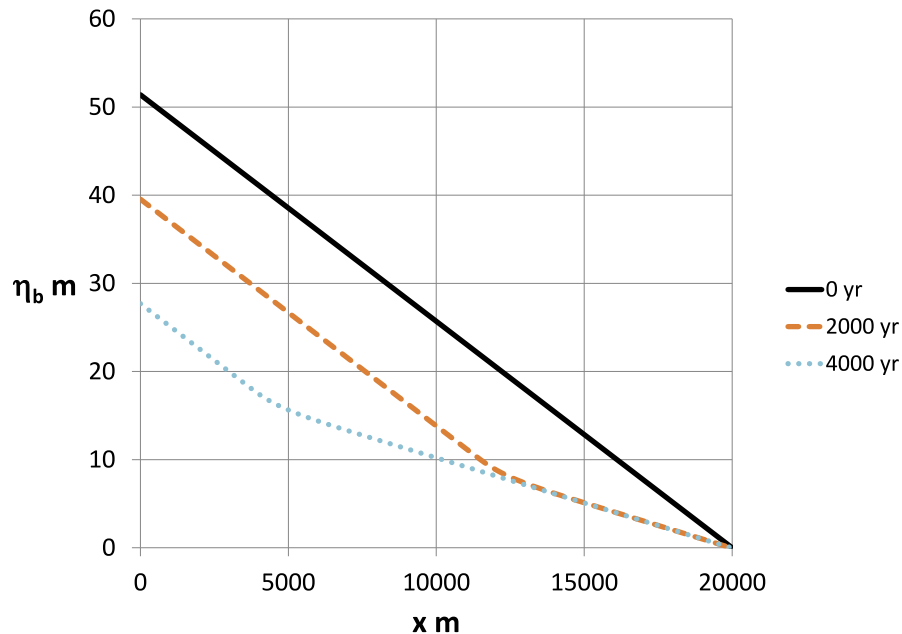


Figure 15. Evolution of an initial bedrock profile to a higher steady-state profile, as predicted by CSA. This figure is the basis for comparison with the results of MRSAA shown in Fig. 16.

Macro-roughness model of bedrock-alluvial river morphodynamics

L. Zhang et al.

Title Page

Abstract

Introduction

Conclusions

References

Tables

Figures

◀

▶

◀

▶

Back

Close

Full Screen / Esc

Printer-friendly Version

Interactive Discussion



Macro-roughness model of bedrock-alluvial river morphodynamics

L. Zhang et al.

Title Page

Abstract

Introduction

Conclusions

References

Tables

Figures

⏪

⏩

◀

▶

Back

Close

Full Screen / Esc

Printer-friendly Version

Interactive Discussion

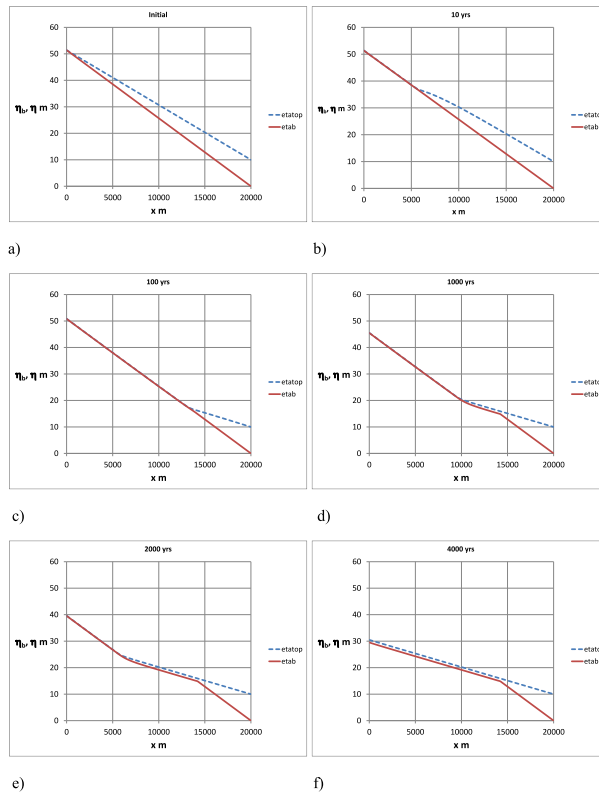


Figure 16. Evolution of bed top and bedrock profiles with an imposed alluvial river mouth at the downstream end and an upstream-migrating bedrock-alluvial transition. The results are for: **(a)** $t = 0$ years; **(b)** $t = 10$ years; **(c)** $t = 100$ years; **(d)** $t = 1000$ years; **(e)** $t = 2000$ years; and **(f)** $t = 4000$ years (steady state). Here **(a)**, **(b)** and **(c)** show the early response, and **(d)**, **(e)** and **(f)** show the late response. All calculations are with MRSAA. A corresponding case using CSA is shown in Fig. 15.